Intelligent Protection of CSC-HVDC Lines Based on Moving Average and Maximum Coordinate Difference Criteria

Intelligent Protection of CSC-HVDC Lines Based on Moving Average and Maximum Coordinate Difference Criteria

Mohammad Farshad*[1], Mazaher Karimi[1]

[1]Department of Electrical Engineering, Faculty of Basic Sciences and Engineering, Gonbad Kavous University, Gonbad Kavous, Iran.

Abstract: Short-circuit fault detection and classification in high-voltage direct-current (HVDC) electric power transmission lines are necessary for rapid location and removal of faults, as well as for recovering all or part of the power transmission capacity. In this study, a new and efficient technique is designed for protecting current-source converter-based HVDC (CSC-HVDC) lines. In this proposed method, new features considering the moving average and maximum coordinate difference criteria are extracted from local voltage and current signals measured with a relatively low sampling rate at the rectifier side. These extracted features provide excellent recognition to distinguish the external and internal short-circuit faults. The multiclass support vector machine model is also used to detect and classify different short-circuit faults in real-time operation. The comprehensive tests on a CSC-HVDC system verify the suggested protection strategy's high accuracy and dependability even under the circumstances not considered in the initial preparing and training stage. These results also authenticate the designed scheme's stability against external

*Address correspondence to Dr. Mohammad Farshad, Department of Electrical Engineering, Faculty of Basic Sciences and Engineering, Gonbad Kavous University, Basirat Blvd., Shahid Fallahi St., Gonbad Kavous 49717-99151, Iran.
https://orcid.org/0000-0002-6631-6636, Tel.: +98 17 3326 6700, E-mail: farshad@gonbad.ac.ir.

faults and lightning strikes, low sensitivity to measurement noises, and excellent performance in detecting and classifying high-resistance internal faults.

Keywords: Current-source converter; HVDC power system; Machine learning; Maximum coordinate difference; Moving average; Transmission line protection.

Abbreviations	
HVDC	high-voltage direct-current
HVAC	high-voltage alternating-current
CSC	current-source converter
VSC	voltage-source converter
CSC-HVDC	CSC-based HVDC
SVM	support vector machine
FIS	fuzzy inference system
SR	smoothing reactor
DCF	dc filter
ECOC	error-correcting output codes
p-g	positive-pole-to-ground
n-g	negative-pole-to-ground
p-n-g	positive-pole-to-negative-pole-to-ground
p-n	positive-pole-to-negative-pole
FDTD	fault detection time delay
SNR	signal-to-noise ratio

Symbols	
V_p	positive pole voltage signal in front of SR
V_n	negative pole voltage signal in front of SR

I_p^{DCF}	positive pole DCF current signal
I_n^{DCF}	negative pole DCF current signal
t	time
N	number of samples in a time window
τ	length of time window
V_{Rated}	rated voltage
I_{Rated}	rated current
fe_1	first input feature extracted using (1)
fe_2	second input feature extracted using (2)
fe_3	third input feature extracted using (3)
fe_4	fourth input feature extracted using (4)
M	number of classes in a multiclass classification problem
m_1	first class in a binary classification problem
m_2	second class in a binary classification problem
W	weight vector
C	soft margin coefficient or box constraint
S	number of training patterns
ε_j	slack variable related to j^{th} training pattern
d_j	binary class label related to j^{th} training pattern
x_j	j^{th} training pattern
B	bias of decision surface/dividing hyperplane
$L(.)$	Lagrange function
α_j	Lagrange coefficient of constraint related to j^{th} training pattern
$\varphi(.)$	mapping function
$K(.,.)$	kernel function
σ	Gaussian kernel scale parameter
k	number of folds in a cross-validation process

1. Introduction

High-voltage direct-current (HVDC) transmission lines may be constructed for various purposes, including bulk power transmission over long distances, power transmission from remote renewable resources (e.g., offshore wind farms), or connection of asynchronous high-voltage alternating-current (HVAC) networks. Two types of converters are generally used for HVDC systems [1]:

■ Current-source converter (CSC)

■ Voltage-source converter (VSC)

Although special attention has recently been paid to the use of VSCs however, most of the existing HVDC systems are founded on CSCs. CSC-based HVDC (CSC-HVDC) systems may have a monopolar or bipolar structure. The bipolar structure usually provides higher reliability and better fault management than the monopolar structure [1]. Fault detection, classification, and identification are vital for accurate location and removal of faults to restore all or part of the power transmission capacity in bipolar CSC-HVDC systems.

Inherent selectivity and sensitivity shortcomings of the traditional protections developed based on the under-voltage, voltage derivative, and current derivative schemes for CSC-HVDC transmission lines [2-5] have motivated new studies in these recent years.

In [5-9], differential protection techniques have been presented and evaluated. The authors in [5] have compensated the capacitive currents distributed along HVDC lines to improve the differential protection's performance during post-fault transients. In [6], the authors have tried to improve the differential protection's operation speed and fault detection accuracy by considering the differential current's polarity in the algorithm. The authors in [7] have eliminated the effect of distributed capacitive currents and improved the differential protection's operation speed by

utilizing the exact line model in the time domain. In [8], the frequency-dependent line model has been used to calculate the transient quantities and improve the differential protection's speed, sensitivity, and selectivity. In [9], the differential protection's performance has been improved by using the distributed line model and eliminating the effect of distributed capacitive currents. Some researchers have also designed pilot plans to protect CSC-HVDC systems' transmission lines [2, 10-14]. In [2], the protection algorithm has been founded on the ratio of transient current and voltage at both line-ends. In [10], the authors have considered the specific frequency current of the filters installed at both line-ends to detect internal faults. The authors in [11] have suggested a directional pilot scheme based on the transient current comparison. In [12], the voltage polarities of the reactors installed at both line-ends have been used to design a pilot protection plan. In [13], the authors have examined the similarity measure of the line and filter current derivatives at both line-ends to identify internal line faults. The authors in [14] have designed a traveling-wave-based pilot protection plan based on the electronic instruments' differential voltage and current signals. Despite the made valuable improvements, the differential and pilot protection plans are more suitable for backup protection since they may not have excellent sensitivity and stability due to the shunt capacitance distributed along long lines. Also, they require the measured signals or computation outputs at both line terminals. These plans often experience operational delays due to the need for transmission of the terminal information. Moreover, their authenticity and correct operation depend on the communication infrastructure's trustworthiness and performance [15].

Some other protection plans have also been designed based on local measurements at one of the HVDC line terminals. In [16], the authors have presented a single-ended protection plan for CSC-HVDC lines considering the quantitative measurement of velocity differences for traveling-waves generated by external and internal faults. The authors in [17] have used the difference of backward

traveling-wave in the event of external and internal faults to detect the faulty section and the voltage fault component's polarity characteristic to determine the faulted line. In [18], the authors have also proposed a single-ended plan established on the traveling-wave theory for protecting two-circuit CSC-HVDC lines. Although these single-ended protection plans [16-18] are promising steps towards increasing the reliability of protection systems and their independence from telecommunication links and related errors, they still have shortcomings that need to be addressed. For example, the authors in [19] have shown that single-ended traveling-wave-based protection plans have lower performance than double-ended ones, especially in dealing with measurement noises. Detection of high-resistance faults is also a common challenge for single-ended traveling-wave-based plans. Moreover, the reviewed single-ended plans [16-18] require a signal sampling frequency of 10 kHz, and their performance is usually highly dependent on this level of sampling frequency. Although this sampling rate may not be too high, compatibility with a lower sampling rate is advantageous for the protection algorithms executed in real-time to monitor the system status continuously. A lower sampling rate will provide more time to perform calculations between two successive samples, facilitating the practical implementation.

In some recent studies, attempts have been made to address some of the shortcomings and design more efficient single-ended protection plans for CSC-HVDC lines with a sampling frequency requirement in the range of 1-2 kHz, relying on the intrinsic capabilities of artificial intelligence. In [20], the authors have proposed a plan for protecting CSC-HVDC lines using the voltage and current samples measured on the rectifier station's ac and dc sides and employing the support vector machine (SVM) classifiers and estimators. However, they have not considered the discrimination ability between external and internal faults in this plan [20]. The authors in [21] have employed the fuzzy inference system (FIS) classifiers to detect and classify faults based on

the current signals measured on the rectifier station's dc side. Although this plan has shown good performance in the conducted tests [21], the regulation of FIS classifiers' parameters and rules is one of its main difficulties. In [22], the author has designed a plan to detect and classify faults in CSC-HVDC lines in one step by employing the k-means clustering algorithm. This plan is also based on single-end data. However, it requires a telecommunication link due to data measured on the inverter station's dc side and the necessity to send the fault detection and classification results to the rectifier station [22].

In this article, a new method is designed to protect bipolar CSC-HVDC lines, relying on artificial intelligence's intrinsic competencies. To this end, it is focused on the extraction of more valuable features and the employment of an appropriate learning model with straightforward training and regulation procedures. The proposed protection plan only requires signals sampled on the rectifier station's dc side at a low frequency of 2 kHz. While the designed method does not need the data transmission link, it has good immunity to measurement disturbances and a promising ability to discriminate between external and internal faults. It also has good generalizability in detecting and classifying internal line faults in one step under the circumstances not seen in the training stage, even high-resistance ones.

In Section 2 of this article, the extracted input features and the employed learning model are introduced. Then, in Section 3, the designed protection plan is presented. The protection plan implementation results on a test HVDC system are provided and discussed in Section 4. This article is eventually concluded in Section 5.

2. Input Features and Learning Model

Any intelligent plan has two fundamental elements: input feature vector and learning model. Here, these elements are introduced for intelligently protecting bipolar CSC-HVDC lines.

2.1. Measurements and Extraction of Useful Features

The structure of a typical bipolar CSC-HVDC transmission system and the designated positions for measuring instruments relative to the smoothing reactor (SR) and dc filter (DCF) of both poles are indicated in Fig. 1. As shown in this figure, only local measurements on the rectifier station's dc side are considered to avoid any need for a telecommunication link in the protection plan. Suppose it is possible to change the current flow direction and displace the converters' operational roles. In that case, the protection plan should be implemented separately on both converter stations. However, only the protection of the rectifier side will always be active. According to Fig. 1, the measurements designated for the protection plan are as follows:

- Positive pole voltage signal in front of SR, V_p
- Negative pole voltage signal in front of SR, V_n
- Positive pole DCF current signal, I_p^{DCF}
- Negative pole DCF current signal, I_n^{DCF}

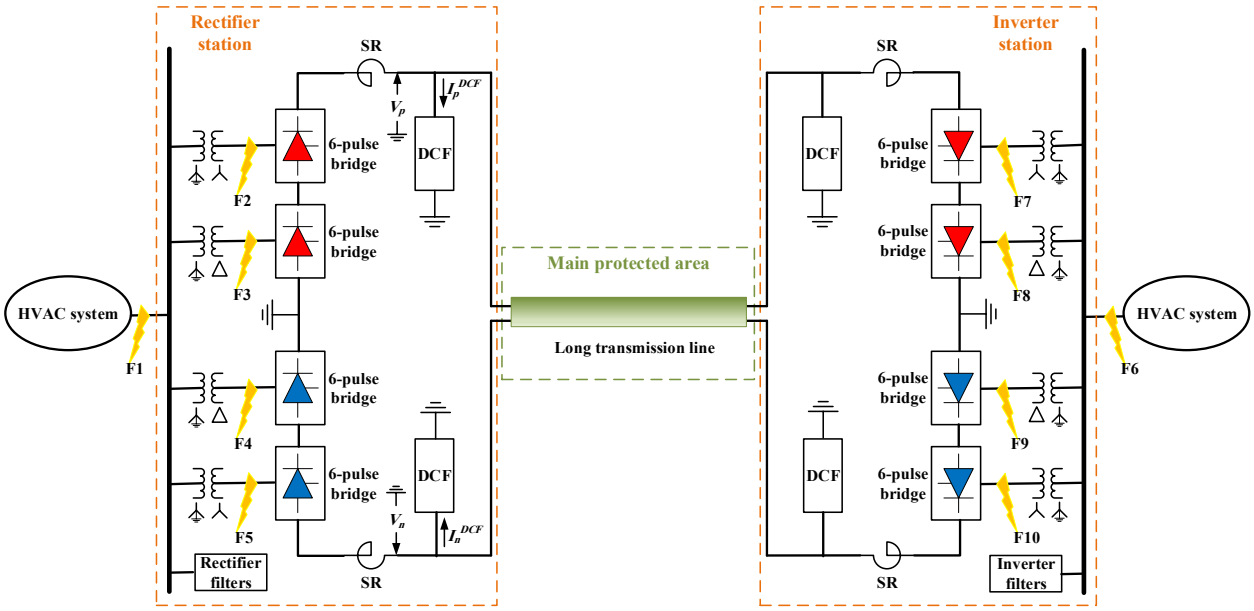

Fig. 1 Typical bipolar CSC-HVDC transmission system and positions of measuring instruments

Four input features for the protection plan at time t are calculated based on 10-ms moving time windows containing N samples from the abovementioned measurements:

$$fe_1[t] = \frac{1}{N \times |V_{Rated}|} \sum_{j=0}^{N-1} V_p\left[t - j\frac{\tau}{N}\right] \tag{1}$$

$$fe_2[t] = \frac{1}{N \times |V_{Rated}|} \sum_{j=0}^{N-1} V_n\left[t - j\frac{\tau}{N}\right] \tag{2}$$

$$fe_3[t] = \frac{1}{|I_{Rated}|} \max_j \left| I_p^{DCF}\left[t - j\frac{\tau}{N}\right]\right|, j = 0,1,\dots,N-1 \tag{3}$$

$$fe_4[t] = \frac{1}{|I_{Rated}|} \max_j \left| I_n^{DCF}\left[t - j\frac{\tau}{N}\right]\right|, j = 0,1,\dots,N-1 \tag{4}$$

where V_{Rated} and I_{Rated} indicate the rated voltage and current of the HVDC system, respectively. Also, τ is the length of time windows (i.e., τ = 10 ms). Based on (1) and (2), it is clear that the first two features (i.e., fe_1 and fe_2) are the moving average [23] of the windowed per-unit voltage signal for the positive and negative poles, respectively. A closer look at (3) and (4) also shows that the

next two features (i.e., fe_3 and fe_4) are equal to the maximum sample value of the windowed per-unit DCF current signal, or in other words, the maximum coordinate difference [24] between the windowed per-unit current signals before and after DCF, for the positive and negative poles, respectively. These four features have been selected after comprehensively inspecting and examining many possible combinations of input features extractable from voltage and current signals sampled with a low rate of 2 kHz at the rectifier station. Indeed, after these inspections and examinations, it was found that with such a low sampling frequency, this proposed set of features is one of the best possible combinations to discriminate between external and internal faults and to detect and classify internal ones in bipolar CSC-HVDC transmission lines. Consider a bipolar CSC-HVDC system with the structure of Fig. 1, a 1000-km long line, and specifications adapted from the CIGRE benchmark system [25]. Fig. 2 exhibits the changes in the proposed input features for internal positive-pole-to-ground (p-g), negative-pole-to-ground (n-g), and positive-pole-to-negative-pole-to-ground (p-n-g) line faults simulated at 1 s with a fault resistance of 25 Ω at a point 335 km away from the rectifier end. Fig. 3 also demonstrates the changes in the proposed input features for external single-phase-to-ground faults simulated at 1 s with a fault resistance of 25 Ω on the ac side of the rectifier and inverter stations.

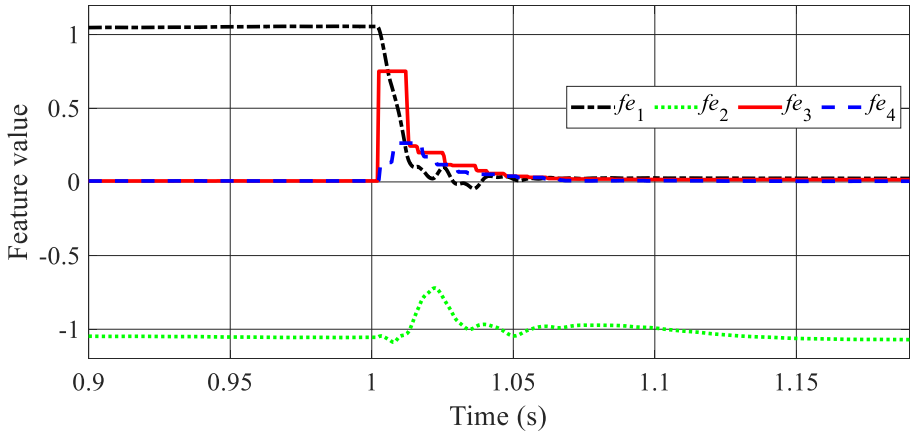

(a)

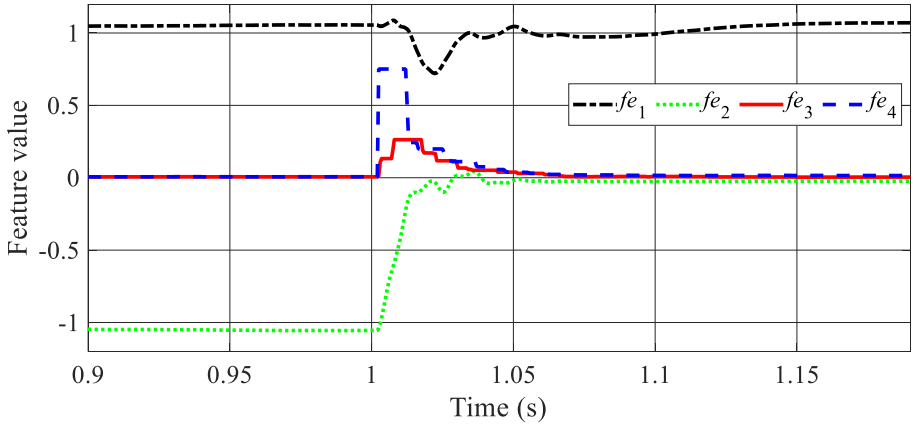

(b)

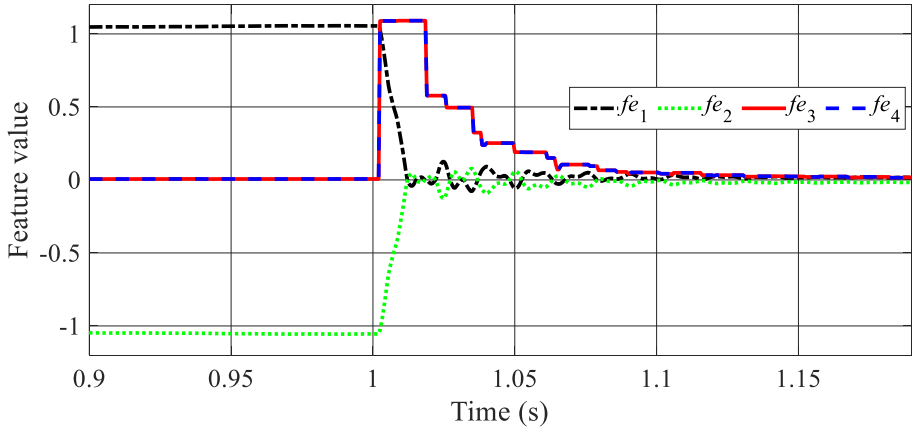

(c)

Fig. 2 Changes in the proposed input features for internal line faults simulated at 1 s with a fault resistance of 25 Ω at a point 335 km away from the rectifier end: a) p-g fault, b) n-g fault, c) p-n-g fault

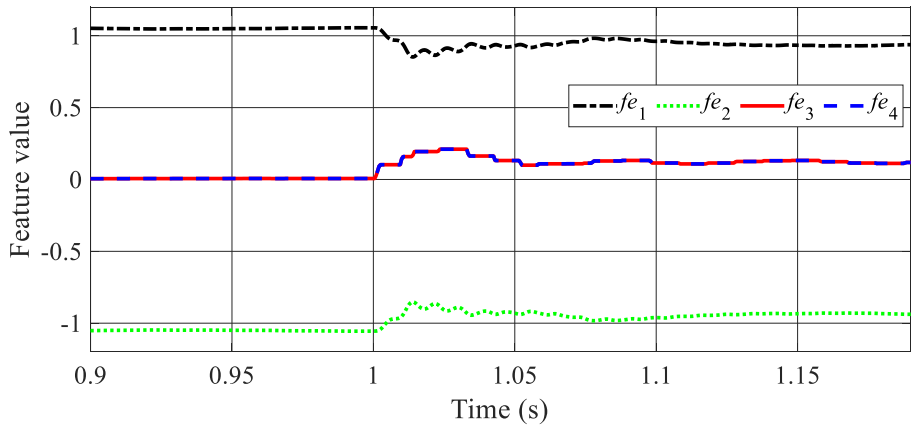

(a)

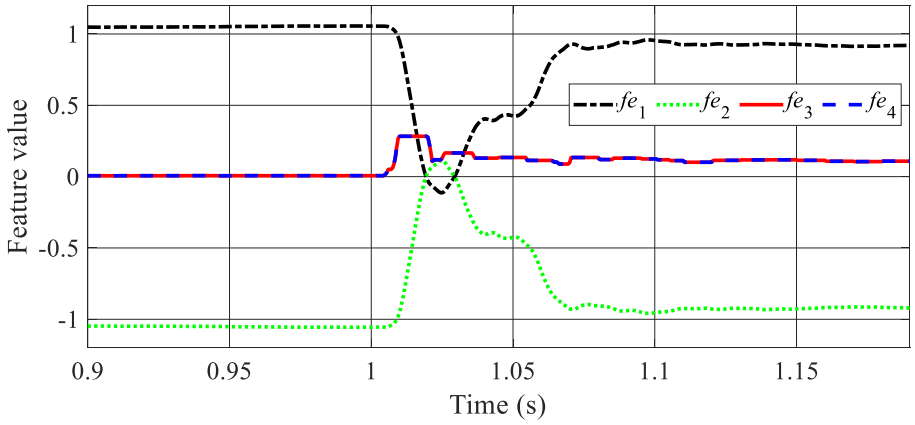

(b)

Fig. 3 Changes in the proposed input features for external single-phase-to-ground faults simulated at 1 s with a fault resistance of 25 Ω: a) on the ac side of the rectifier station, b) on the ac side of the inverter station

By investigating Figs. 2(a) to 2(c), it can be comprehended that the moving averages of positive and negative voltage signals (i.e., fe_1 and fe_2) provide an excellent distinguishing power to detect and classify different types of internal line faults. On the other hand, by comparing Fig. 2(c) with Figs. 3(a) and 3(b), it can be seen that these two first features may not be able to correctly discriminate between internal double-pole faults and external ac-side faults, especially in the early post-fault moments. However, according to these figures, the next two features based on the maximum sample value of DCF current signal or the maximum coordinate difference between

current signals before and after DCF (i.e., fe_3 and fe_4) compensate for this shortcoming and provide adequate distinguishing power for these conditions.

2.2. Machine-Learning Model

Employing an appropriate machine-learning model is of great importance in the methods based on artificial intelligence. One of the most effective learning models for classification problems is the SVM model. This learning model is rooted in the statistical learning theory and founded on the structural risk minimization principle [26]. The SVM learning model provides a balance between accuracy and generalizability by dividing patterns of different classes with the least possible error and the maximum confidence margin.

The SVM learning model was first developed for binary classification problems and then extended for multiclass ones. In this article, the multiclass version of SVM is employed for intelligently protecting bipolar CSC-HVDC lines. In this multiclass version, if there are M classes in the set of training patterns, $M\times(M\text{-}1)/2$ binary SVM classifiers are formed using the patterns of each different pair of classes, i.e., with the one-against-one coding design. When a new unseen pattern is presented to this multiclass classifier, a class is selected as the output that minimizes the aggregation of binary losses for the constituent binary classifiers, i.e., based on the error-correcting output codes (ECOC) model [27].

The learning process of each binary SVM classifier involves solving the following convex optimization problem to reach the decision surface/dividing hyperplane of training patterns with two classes, m_1 and m_2 [28]:

$$\min_{W,\varepsilon_j} \frac{1}{2}\|W\|^2 + C\sum_{j=1}^{S}\varepsilon_j \qquad (5-a)$$

Subject to:

$$d_j \times \left(W^T \times x_j + B\right) \geq 1 - \varepsilon_j, \qquad for\ j = 1,2,\dots,S \tag{5-b}$$

$$\varepsilon_j \geq 0, \qquad for\ j = 1,2,\dots,S \tag{5-c}$$

where W is the weight vector, C indicates the soft margin coefficient or box constraint, S stands for the number of training patterns, ε_j is the slack variable related to the j^{th} training pattern (for controlling noisy or linearly non-separable data), d_j is the binary class label related to the j^{th} training pattern (equal to 1 for m_1 and -1 for m_2), x_j stands for the j^{th} training pattern, and B represents the bias of decision surface/dividing hyperplane. The dual of the optimization problem (5) based on the Lagrange function $L(\alpha)$ and Karush-Kuhn-Tucker conditions are as follows [28]:

$$\max_{\alpha} L(\alpha) = \sum_{j=1}^{S} \alpha_j - \frac{1}{2} \sum_{j,h=1}^{S} \alpha_j \times \alpha_h \times d_j \times d_h \times x_j^T \times x_h \tag{6-a}$$

Subject to:

$$0 \leq \alpha_j \leq C, \qquad for\ j = 1,2,\dots,S \tag{6-b}$$

$$\sum_{j=1}^{S} d_j \times \alpha_j = 0 \tag{6-c}$$

where α_j is the Lagrange coefficient of the constraint related to the j^{th} training pattern. The optimal solution to the optimization problem (5) can be achieved by solving this dual problem. However, the decision surface/dividing hyperplane obtainable from the abovementioned formulations is linear. Hence, a kernel function is usually used to achieve a nonlinear decision surface/dividing hyperplane. The dual optimization problem (6) can be rewritten as follows, based on the mapping $x_j \to \varphi(x_j)$ and the kernel function $K(x_j, x_h) = \varphi^T(x_j) \times \varphi(x_h)$ [28]:

$$\max_{\alpha} L(\alpha) = \sum_{j=1}^{S} \alpha_j - \frac{1}{2} \sum_{j,h=1}^{S} \alpha_j \times \alpha_h \times d_j \times d_h \times K(x_j, x_h) \tag{7-a}$$

Subject to:

$$0 \le \alpha_j \le C, \qquad for\ j = 1,2,\dots,S \tag{7-b}$$

$$\sum_{j=1}^{S} d_j \times \alpha_j = 0 \tag{7-c}$$

One of the most widely used and efficient kernel functions is the Gaussian kernel. This kernel can be defined as follows:

$$K(x_j, x_h) = \exp\left(-\frac{\|x_j - x_h\|^2}{\sigma^2}\right) \tag{8}$$

where σ indicates the Gaussian kernel scale parameter.

3. Designed Protection Plan

In the protection plan of this article, at any moment, the four features introduced in Section 2.1 are extracted from 10-ms moving time frames of the measured voltage and DCF current samples and formed as the input pattern. Then, this input pattern is presented to the multiclass SVM classifier with the Gaussian kernel function described in Section 2.2. The corresponding class is determined based on the set of binary SVM classifiers and the ECOC model. According to Section 2.2, for four possible output classes, six binary SVM classifiers are required in the one-against-one coding design of the multiclass SVM classifier. Fig. 4 provides an outline of the proposed protection plan in real-time operation.

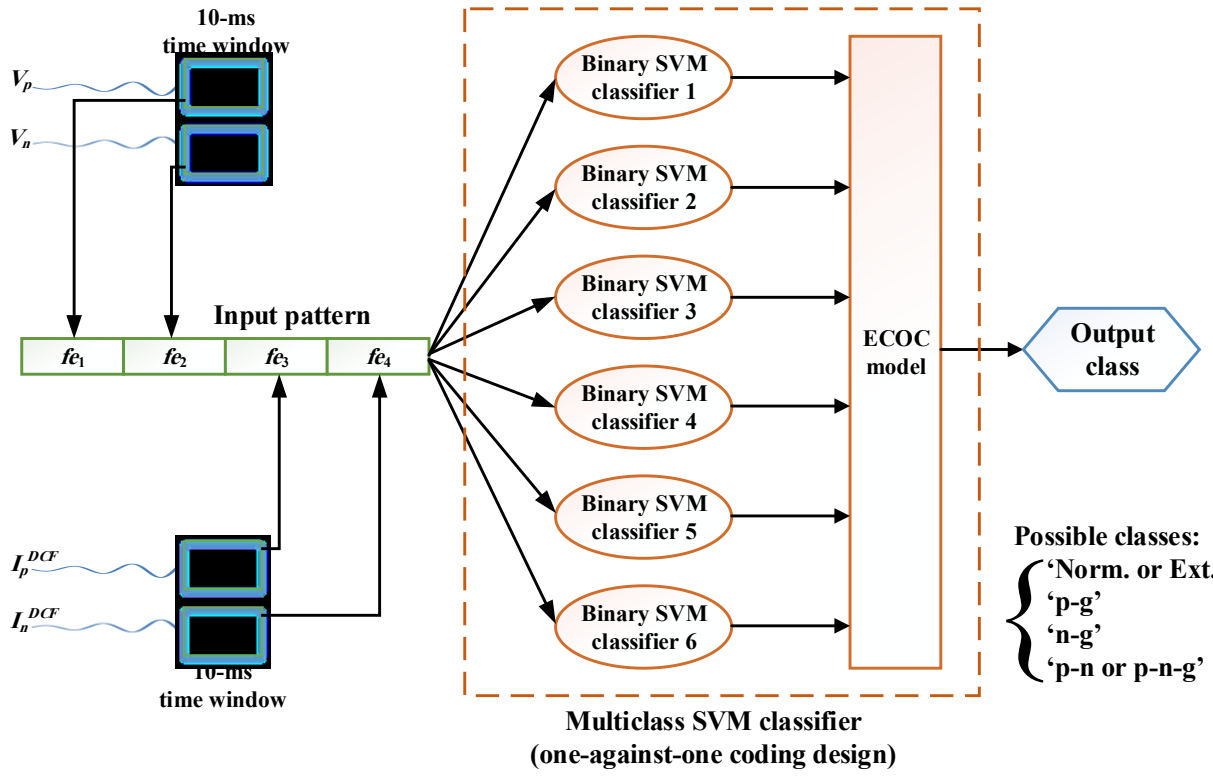

Fig. 4 Outline of the proposed real-time protection plan

At any moment, one of the following four possible classes can be selected as the output class of the proposed protection plan:

- Normal condition or external fault, 'Norm. or Ext.'

- Internal p-g fault, 'p-g'

- Internal n-g fault, 'n-g'

- Internal positive-pole-to-negative-pole (p-n) or p-n-g fault, 'p-n or p-n-g'

Whenever the protection algorithm detects one type of internal fault, the protection output remains unchanged until it is reset.

The SVM classifier in the proposed plan should first be prepared and trained through an offline process before being used in real-time. The offline preparing and training process includes the following main steps:

1) A set of training patterns is produced by precisely simulating the HVDC system under different fault and normal conditions. In fault conditions, each training pattern includes the introduced input features extracted from 10-ms data frames of the post-fault voltage and DCF current samples. In normal conditions without faults, the patterns' features can be extracted from any 10-ms data frames of the voltage and DCF current samples. In the phase of generating the training pattern set, any issue which is a concern can be included in the conditions.
2) The SVM hyperparameters (i.e., C and σ) are adjusted via a k-fold cross-validation process and based on the Bayesian optimization, minimizing the cross-validation loss.
3) Finally, the SVM classifier is trained using all the training patterns and the selected values for the SVM hyperparameters. This classifier is ready to be used in the protection plan in real-time.

Proper implementation of the above preparation and training steps will lead to the desired performance of the proposed protection plan. In contrast, improper execution of the above offline steps will degrade the performance. For example, selecting inappropriate values for the SVM hyperparameters will reduce the internal fault detection accuracy, reduce the stability against external faults, and increase the response time due to the increased validation loss and decreased generalization power.

4. Results and Discussion

In this section, for assessing the designed protection plan's performance, the test transmission system of Fig. 1 is modeled in PSCAD/EMTDC [29] with specifications adapted from the CIGRE

benchmark system [25]. The modeled test system has a nominal voltage of ±500 kV and a nominal transmission capacity of 2000 MW. This bipolar system's overhead line is 1000 km long, modeled with the frequency-dependent parameters based on the arrangement shown in Fig. 5 [30]. The voltage and current signals' sampling rate in the simulated system is 2 kHz. The proposed protection plan is realized in MATLAB [31] and examined with the signals acquired from the simulation.

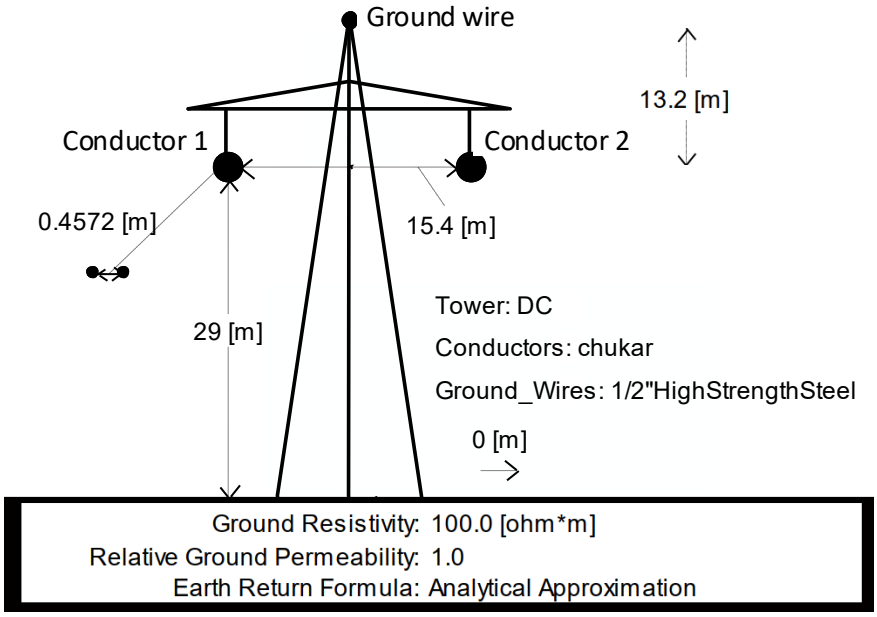

Fig. 5 Arrangement of the transmission line modeled in PSCAD/EMTDC

4.1. Preparing and Training

For preparing the protection plan, a set of training patterns should first be generated by simulating the test CSC-HVDC system under different conditions. These conditions are provided in Table 1. Each training pattern includes the four features described in Section 2.1 (i.e., fe_1, fe_2, fe_3, and fe_4), extracted from 10-ms data frames of the measured voltage and DCF current samples. In the fault

conditions, the starting point of these data windows is the moment of fault signature appearance at the terminal. However, there is no specific requirement for the starting point of these data windows in the normal conditions without faults.

Table 1 Conditions for generating the set of training patterns

Condition	Fault type	Fault location	Fault resistance	Load current	Fault inception angle	Number of patterns
Internal dc faults	p-g, n-g, p-n, p-n-g	From 1% to 99% of the line length with a step of 7%	0.01 Ω, 50 Ω, 100 Ω, 150 Ω, 200 Ω, 300 Ω, 500 Ω	500 A, 1200 A, 1900 A	Not applicable	1260
External ac faults	11 ac fault types involving the ground and the phases a, b, and c	F1, F2, F3, F4, F5, F6, F7, F8, F9, F10 (according to Fig. 1)	0.01 Ω, 50 Ω, 100 Ω, 200 Ω, 300 Ω	500 A, 1200 A, 1900 A	45°, 135°, 225°, 315°	6600
Normal conditions	Not applicable	Not applicable	Not applicable	500 A, 1200 A, 1900 A	Not applicable	3

According to the conditions of Table 1, a total of 7863 training patterns are formed, each labeled as one of the four possible classes mentioned in Section 3. These training patterns should be used to train the multiclass SVM classifier and regulate its hyperparameters. The box constraint C and the Gaussian kernel scale σ are adjusted via a 5-fold cross-validation process and based on the Bayesian optimization, minimizing the cross-validation loss. Fig. 6 shows the loss changes during the optimization process in terms of the SVM hyperparameters. Based on the model obtained for the objective function, the best estimations for C and σ are 35.45 and 0.4, respectively. The multiclass SVM classifier is eventually trained using the complete training pattern set and considering these hyperparameters values.

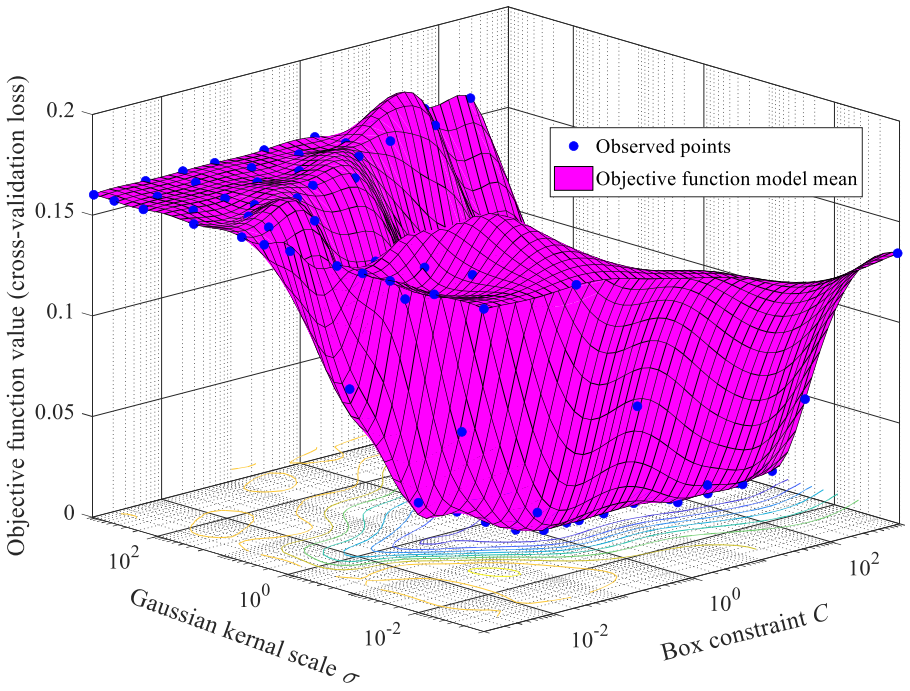

Fig. 6 Cross-validation loss in terms of the SVM hyperparameters

4.2. Performance for Internal Faults

Here, the test CSC-HVDC system is simulated under various internal fault conditions, as different as possible from the conditions of training patterns. These test conditions are as follows:

- Fault type: p-g, p-n, and p-n-g

- Fault location: at random distances including 1.2%, 7.1%, 13.7%, 20.3%, 26.9%, 33.5%, 40.1%, 46.7%, 53.3%, 59.9%, 66.5%, 73.1%, 79.7%, 86.3%, 92.9%, and 99.5% of the line length from the rectifier station

- Fault resistance: 5 Ω, 25 Ω, 75 Ω, 125 Ω, 175 Ω, 250 Ω, 350 Ω, 400 Ω, and 450 Ω

- Load current: 700 A, 1000 A, 1400 A, and 1700 A

According to the above conditions, the suggested protection plan is tested for the combinations of 3 fault types, 16 fault locations, 9 fault resistances, and 4 load currents, i.e., for a total of 1728

unseen internal fault cases. Tables 2 and 3 present the test results regarding the various fault resistances for the p-g and double-pole (i.e., p-n and p-n-g) faults, respectively. In these tables, the fault detection time delay (FDTD) has been calculated from the moment of fault signature appearance at the terminal.

Table 2 Results in terms of various fault resistances for internal p-g faults

Fault resistance	Number of test cases	Percentage of correct detection and classification	Minimum FDTD (ms)	Maximum FDTD (ms)	Average FDTD (ms)
5 Ω	64	100%	3	9	4.4
25 Ω	64	100%	3	11.5	4.6
75 Ω	64	100%	3	8.5	4.4
125 Ω	64	100%	3	7.5	4.3
175 Ω	64	100%	2.5	8.5	4.3
250 Ω	64	100%	2.5	9.5	4.3
350 Ω	64	100%	2.5	21.2	5.1
400 Ω	64	100%	2.8	42.7	6.1
450 Ω	64	100%	3	47.9	7.8
Total	576	100%	2.5	47.9	5.0

Table 3 Results in terms of various fault resistances for internal double-pole (i.e., p-n and p-n-g) faults

Fault resistance	Number of test cases	Percentage of correct detection and classification	Minimum FDTD (ms)	Maximum FDTD (ms)	Average FDTD (ms)
5 Ω	128	100%	3.5	21.0	6.3
25 Ω	128	100%	3.0	12.0	5.7
75 Ω	128	100%	3.0	8.5	5.0
125 Ω	128	100%	3.0	8.0	4.6
175 Ω	128	100%	3.2	7.0	4.3
250 Ω	128	100%	3.2	6.1	4.1
350 Ω	128	100%	3.3	6.5	4.6
400 Ω	128	100%	3.5	7.5	5.0
450 Ω	128	100%	3.5	8.5	5.5
Total	1152	100%	3.0	21.0	5.0

As can be comprehended from Tables 2 and 3, in all the 1728 unseen internal fault cases, the presented protection plan has quickly detected and correctly classified the solid and high-resistance line faults. According to the results provided for the single-pole faults in Table 2, the average FDTD is less than 6.5 ms for the fault resistances up to 400 Ω. However, it slightly increases to 7.8 ms at the fault resistance of 450 Ω. On the other hand, the results provided for the double-pole faults in Table 3 reveal that the average FDTD is below 6.5 ms for all the fault resistances. It is worth noting that the presented protection plan has not malfunctioned during the pre-fault moments of these test cases.

Fig. 7 represents the average FDTD regarding the various fault locations for the p-g and double-pole (i.e., p-n and p-n-g) faults. As can be understood from this figure, the average FDTD has slightly increased for the single-pole faults near the remote line terminal and reached 10.7 ms at a distance of 99.5% of the line length from the rectifier station.

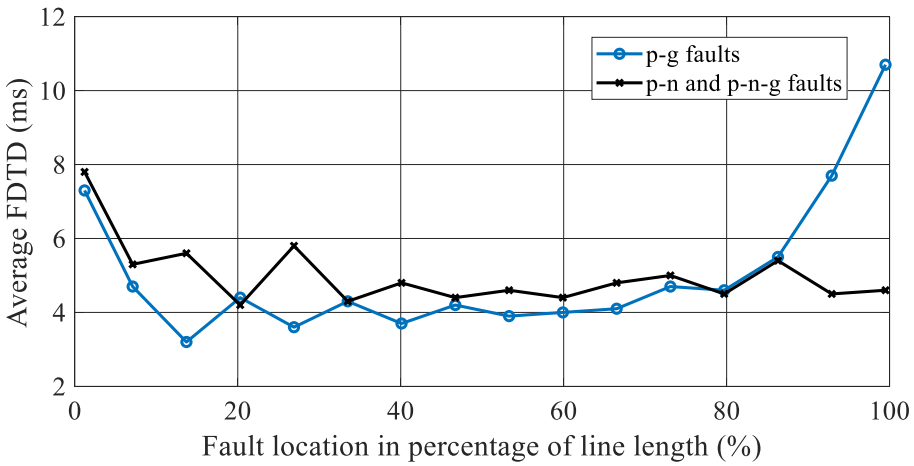

Fig. 7 Average FDTD in terms of various locations for internal line faults

As examples of the correct operation in real-time, Fig. 8 exhibits the changes in the input features and output class of the protection algorithm for p-g and p-n-g faults simulated at 1 s with a resistance of 450 Ω and a pre-fault current of 1700 A at a point 863 km away from the rectifier end.

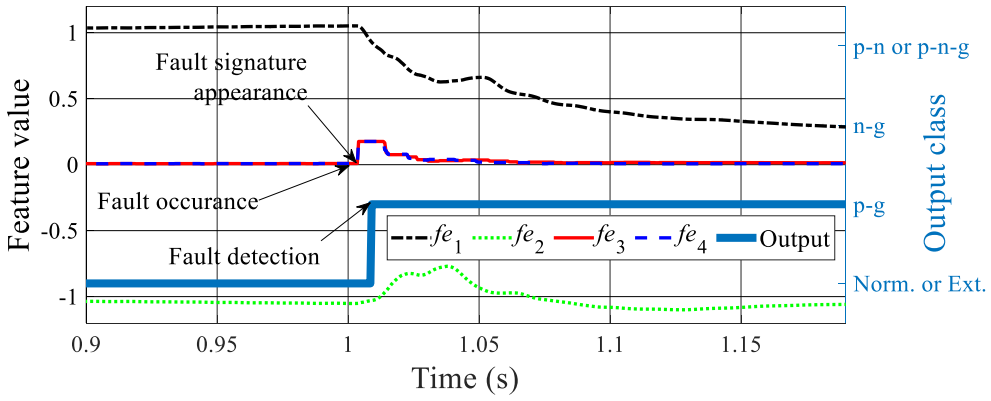

(a)

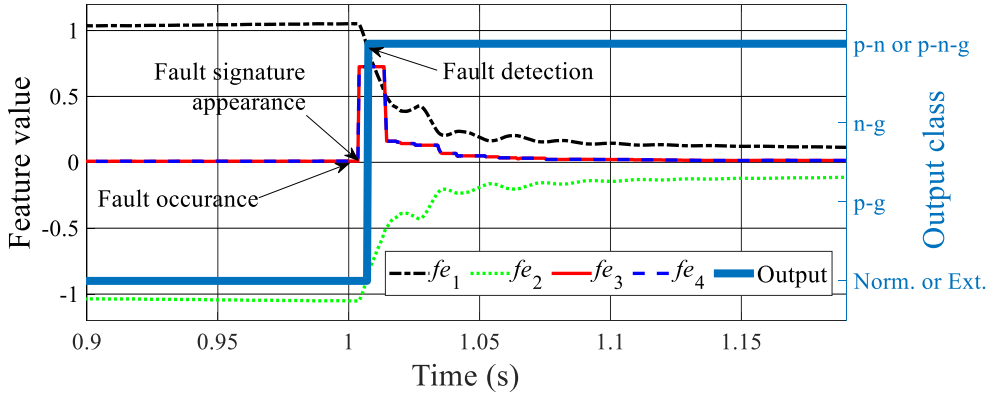

(b)

Fig. 8 Changes in the input features and output class of the proposed algorithm for internal line faults simulated at 1 s with a resistance of 450 Ω and a pre-fault current of 1700 A at a point 863 km away from the rectifier end: a) p-g fault, b) p-n-g fault

4.3. Performance for External Faults in HVAC Systems

In this section, the test system is simulated under various external faults in the connected HVAC systems, with conditions as different as possible from those considered for generating the training patterns. These test conditions are as follows:

- Fault type: 11 ac fault types involving the ground and phases a, b, and c

- Fault location: F1 and F6 (according to Fig. 1)

- Fault resistance: 5 Ω, 25 Ω, 75 Ω, 150 Ω, and 250 Ω

- Load current: 700 A, 1000 A, 1400 A, and 1700 A

- Fault inception angle: 0^{o}, 90^{o}, 180^{o}, and 270^{o}

According to the above conditions, the proposed plan is evaluated for the combinations of 11 fault types, 2 fault locations, 5 fault resistances, 4 load currents, and 4 fault inception angles, i.e., for a total of 1760 unseen external fault cases. The performance evaluation results for the various types of external faults in the connected HVAC systems are presented in Table 4. Based on these results, the protection plan has been stable against 99.375% of the 1760 unseen external fault cases. It has malfunctioned only in few phase-to-phase faults in the HVAC system connected to the rectifier station. Indeed, the SVM classifier has misclassified only 11 out of 480 external phase-to-phase fault cases as 'p-n or p-n-g' due to the real-time position of the feature vector relative to the SVM's decision surface/dividing hyperplane, while it has remained entirely stable against other external fault types. This little accuracy sacrifice in the case of external faults is acceptable given the fact that the relevant test conditions were not considered in the training stage (i.e., unseen test conditions), confirming the plan's good generalizability. It is worth noting that in these results, the same probability of occurrence has been considered for different types of ac faults, while double-phase faults are less likely to occur than single-phase faults.

Table 4 Results for various types of external faults in the connected HVAC systems

Fault location	Fault type	Number of test cases	Percentage of correct detection and classification as 'Norm. or Ext.'	Percentage of incorrect detection and classification as an internal dc fault
F1	**a-g**	80	100%	0%
	b-g	80	100%	0%
	c-g	80	100%	0%
	a-b-g	80	100%	0%
	a-c-g	80	100%	0%
	b-c-g	80	100%	0%
	a-b-c-g	80	100%	0%
	a-b	80	95%	5%
	a-c	80	96.25%	3.75%
	b-c	80	95%	5%
	a-b-c	80	100%	0%
F6	**a-g**	80	100%	0%
	b-g	80	100%	0%
	c-g	80	100%	0%
	a-b-g	80	100%	0%
	a-c-g	80	100%	0%
	b-c-g	80	100%	0%
	a-b-c-g	80	100%	0%
	a-b	80	100%	0%
	a-c	80	100%	0%
	b-c	80	100%	0%
	a-b-c	80	100%	0%
Total		1760	99.375%	0.625%

4.4. Performance under Measurement Noises

There are several technologies for measuring voltage and current signals in HVDC systems [32]. The proposed protection plan is not limited to a specific measuring technology. However, different measuring technologies may have different accuracy and performance. Hence, to ensure the applicability of the proposed protection plan with various measuring technologies, its performance is investigated under different levels of measurement non-ideality. In this regard, the white Gaussian noise is added to the voltage and DCF current signals acquired under test conditions. The input features are extracted and presented to the same previously trained SVM classifier. Table 5 presents the performance test results regarding the various signal-to-noise ratios (SNRs) for the internal fault cases of Section 4.2 and the external fault cases of Section 4.3. According to these results, the fault detection and classification accuracy has been satisfactory under reasonable noise levels, even with an SNR of 20 dB. However, for a higher noise level with an SNR of 15 dB, the proposed plan's stability against the external faults has decreased significantly. These results should be taken into account when selecting and designing the measurement chains.

Table 5 Results in terms of various noise levels for internal and external faults

	Internal p-g faults		**Internal double-pole (i.e., p-n and p-n-g) faults**		**External faults in the HVAC systems**	
SNR	**Number of test cases**	**Percentage of correct detection and classification**	**Number of test cases**	**Percentage of correct detection and classification**	**Number of test cases**	**Percentage of correct detection and classification as 'Norm. or Ext.'**
∞ dB (ideal)	576	100%	1152	100%	1760	99.375%
35 dB	576	100%	1152	100%	1760	99.205%
30 dB	576	100%	1152	100%	1760	99.091%
25 dB	576	100%	1152	100%	1760	99.034%
20 dB	576	100%	1152	100%	1760	97.102%
15 dB	576	82.292%	1152	85.330%	1760	29.375%

4.5. Competence of the Selected Features

As stated in Section 2.1, the four features (i.e., fe_1, fe_2, fe_3, and fe_4) are extracted to form the input pattern in the proposed protection plan. The first two features (i.e., fe_1 and fe_2) are extracted from the measured voltage signals, and the next two features (i.e., fe_3 and fe_4) are extracted from the measured DCF current signals. Here, all the steps of hyperparameter regulation, training, and performance evaluation, similar to Sections 4.1 to 4.3, are repeated using only the voltage features (i.e., fe_1 and fe_2) and only the current features (i.e., fe_3 and fe_4). Table 6 provides the performance evaluation results in these cases compared to the recommended case using all four features. It should be noted that the adjusted values for C and σ in the case of using only the voltage features are 1.62 and 0.04, respectively, and in the case of using only the current features are 312.19 and 0.04, respectively.

Table 6 Results considering different combinations of input features

	Internal p-g faults		**Internal double-pole (i.e., p-n and p-n-g) faults**		**External faults in the HVAC systems**	
Input features	**Number of test cases**	**Percentage of correct detection and classification**	**Number of test cases**	**Percentage of correct detection and classification**	**Number of test cases**	**Percentage of correct detection and classification as 'Norm. or Ext.'**
***fe*$_1$, *fe*$_2$, *fe*$_3$, and *fe*$_4$**	576	100%	1152	100%	1760	99.375%
***fe*$_1$ and *fe*$_2$**	576	100%	1152	100%	1760	**70.227%**
***fe*$_3$ and *fe*$_4$**	576	**68.750%**	1152	98.351%	1760	95.568%

As comprehendible from Table 6, the use of only fe_1 and fe_2 leads to a decrease in the protection plan's stability against the external ac faults compared to the recommended base case. Also, using only fe_3 and fe_4 significantly reduces the detection and classification accuracy for the internal

single-pole faults. Indeed, these results confirm the analysis of Section 2.1 regarding the necessity to use all the four recommended features in the input pattern.

4.6. Performance for Lightning Strikes

Here, to further investigate the proposed plan's stability against the induced transients from other external events, the lightning strike on the ground wire at a distance of 10 km from the rectifier station at 0.8 s is simulated in PSCAD/EMTDC based on the guidelines provided in [33]. Three towers with a 400-m span on each side of the lightning strike point are modeled with a surge impedance of 150 Ω and a foot resistance of 25 Ω. The lightning current surge is generated with a peak value of 200 kA, a front time of 10 μs, and a time to half-value of 350 μs [34] (as shown in Fig. 9).

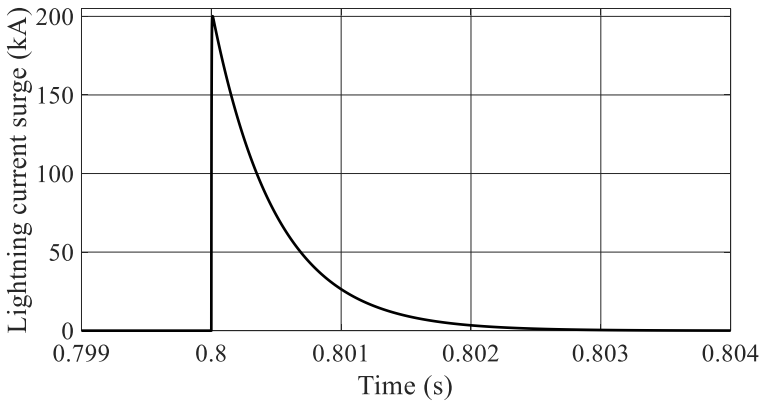

Fig. 9 The lightning current surge struck on the ground wire (200 kA and 10/350 μs)

Fig. 10 presents the changes in the input features and output class of the protection algorithm. As can be comprehended from this figure, the features have not changed significantly, and consequently, the proposed algorithm has remained stable during the transients induced due to the lightning strike.

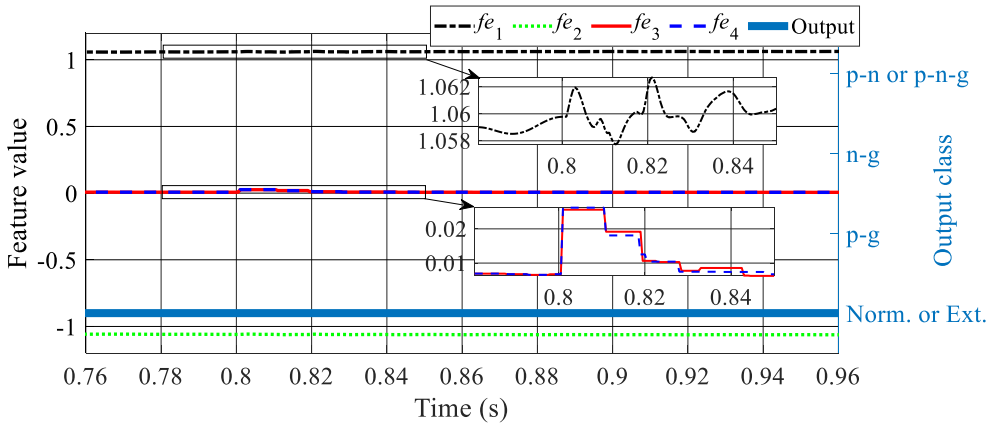

Fig. 10 Changes in the input features and output class of the proposed algorithm in dealing with the transients induced due to the lightning strike on the ground wire at 0.8 s

In some cases, a smaller lightning surge may escape the shelter provided by the ground wire and directly strike on the pole conductor [33]. Hence, two lightning strikes on the positive and negative pole conductors at a distance of 10 km from the rectifier station at 0.8 s are also simulated in the test system, considering surge arresters installed in front of DCFs. The relevant lightning current surge is generated with a peak value of 15 kA, a front time of 1.2 μs, and a time to half-value of 50 μs [34] (as shown in Fig. 11).

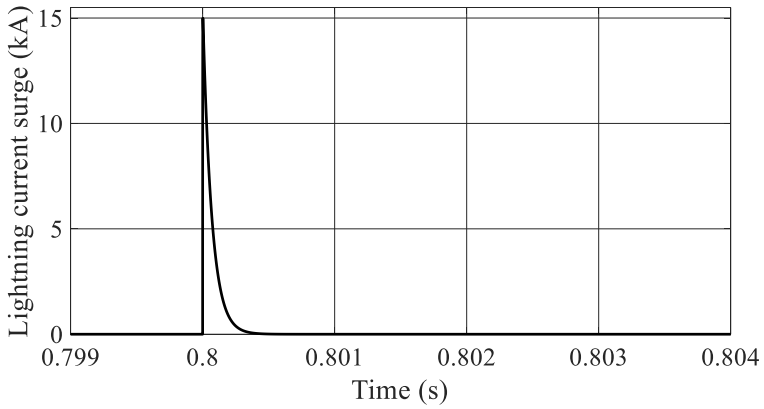

Fig. 11 The lightning current surge struck on the pole conductors (15 kA and 1.2/50 μs)

Figs. 12 and 13 show the measured voltage and DCF current signals for the direct lightning strikes on the positive and negative pole conductors. Fig. 14 also presents the changes in the input features and output class of the protection algorithm in these cases. As shown in this figure, the features extracted based on the average voltage (i.e., fe_1 and fe_2) have not changed significantly, and consequently, the proposed algorithm has not malfunctioned during the transients generated due to the direct lightning strikes.

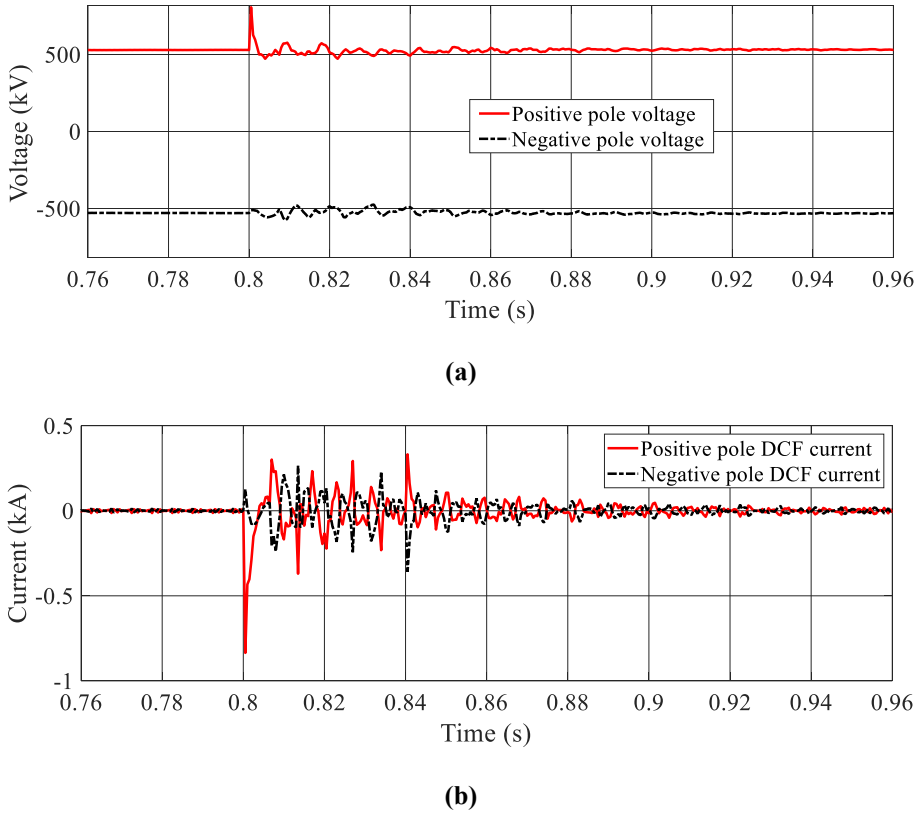

Fig. 12 Measured signals for the lightning strike on the positive pole conductor at 0.8 s: a) voltage, b) DCF current

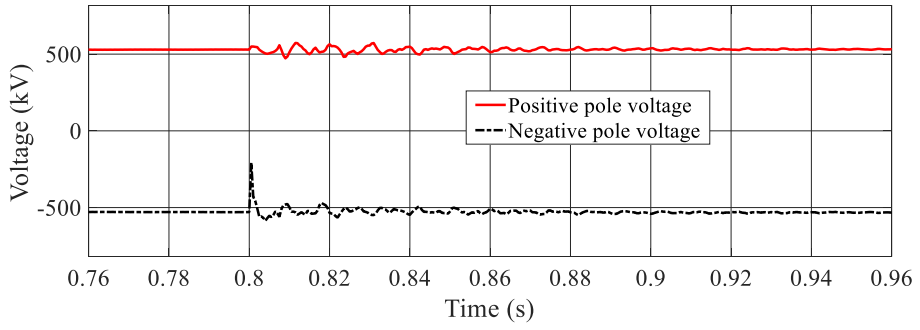

(a)

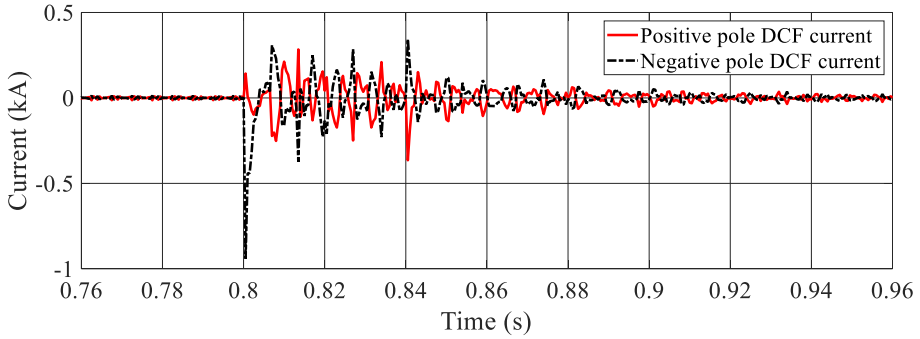

(b)

Fig. 13 Measured signals for the lightning strike on the negative pole conductor at 0.8 s: a) voltage, b) DCF current

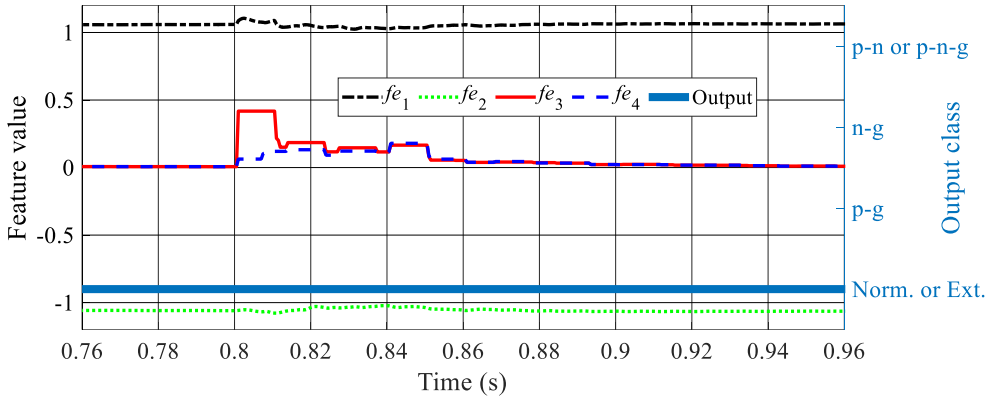

(a)

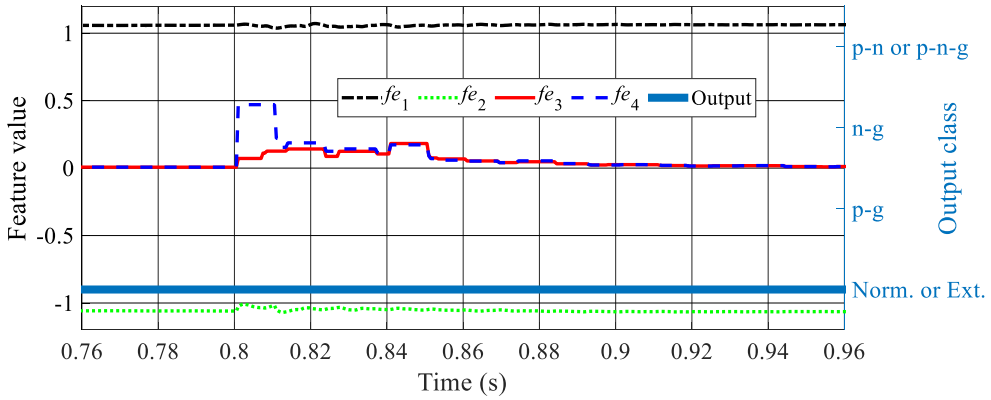

(b)

Fig. 14 Changes in the input features and output class of the proposed algorithm in dealing with the lightning strike at 0.8 s: a) on the positive pole, b) on the negative pole

4.7. Performance for Pole Conductor Interruptions

Here, to investigate the proposed plan's performance in the case of conductor interruption, three following interruption scenarios (as also illustrated in Fig. 15) are simulated for the positive pole at a distance of 400 km from the rectifier station at 0.8 s:

1) Both sides contact the ground with high resistance of 500 Ω

2) Only the inverter side contacts the ground with high resistance of 500 Ω

3) Only the rectifier side contacts the ground with high resistance of 500 Ω

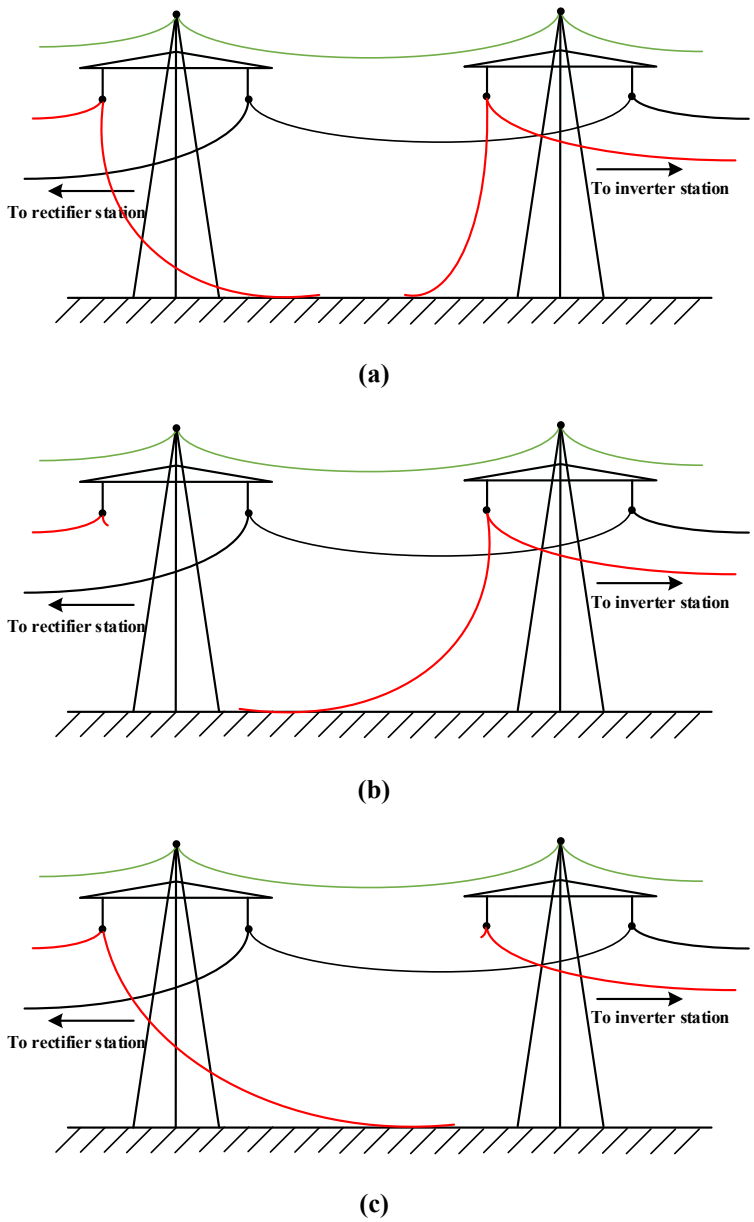

Fig. 15 Three conductor interruption scenarios: a) both sides contact the ground, b) only the inverter side contacts the ground, c) only the rectifier side contacts the ground

Fig. 16 displays the changes in the input features and output class of the protection algorithm in these scenarios. As can be understood from this figure, the suggested plan has detected all the pole interruption events. However, when the rectifier side has not contacted the ground (i.e., in Scenario 2), the positive pole interruption has been misclassified as a negative pole's fault. The proposed

plan's performance in dealing with the pole interruption scenarios should be considered when employing it.

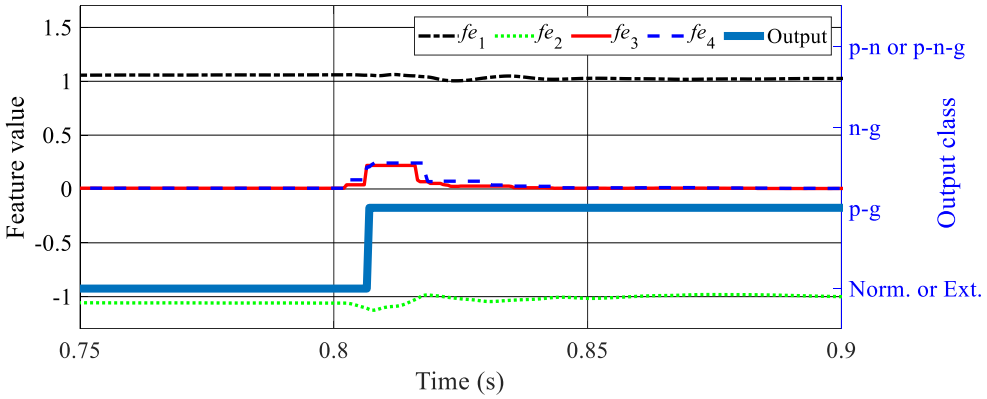

(a)

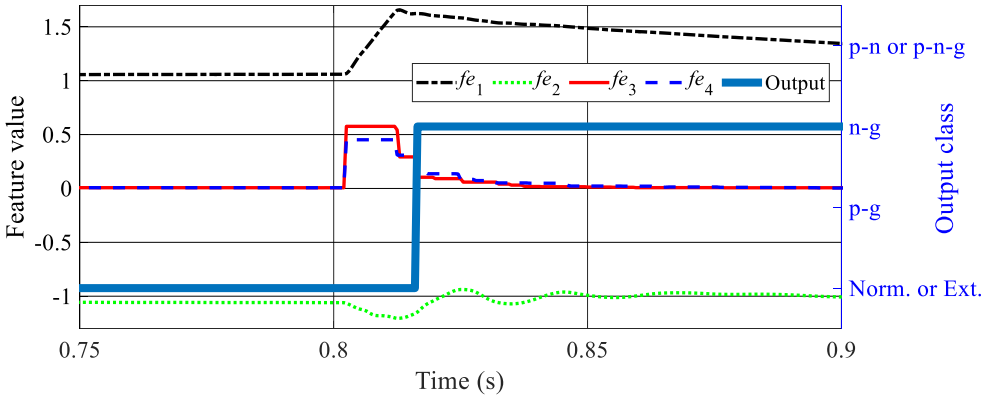

(b)

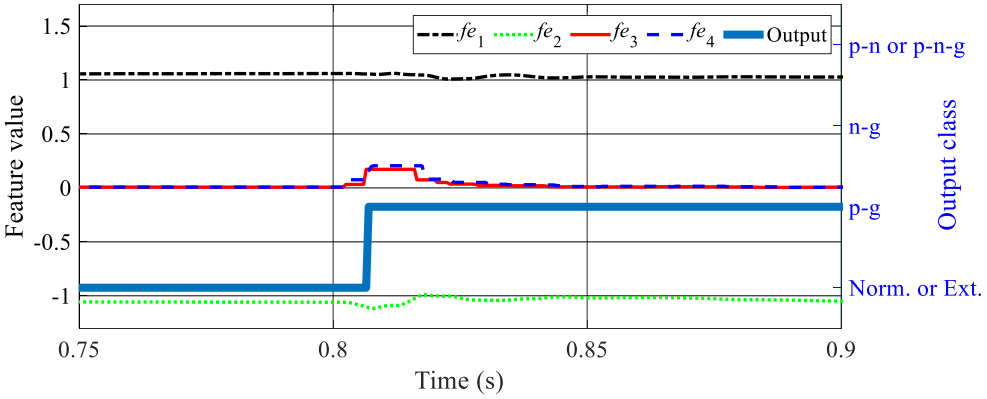

(c)

Fig. 16 Changes in the input features and output class of the proposed algorithm for the positive pole interruption at a distance of 400 km at 0.8 s: a) in Scenario 1, b) in Scenario 2, c) in Scenario 3

4.8. Effect of DCF Disconnection

If one or both DCFs are disconnected, the proposed plan cannot work correctly since the disconnected DCF's current and relevant feature will be permanently zero according to (3) and (4). However, based on the results provided in Section 4.5 and Table 6, the proposed plan is also applicable using only the voltage features (i.e., fe_1 and fe_2), sacrificing 30% stability against external faults. Therefore, a backup plan with less stability can be prepared using only the voltage features (i.e., fe_1 and fe_2) and utilized in the case of DCF disconnection.

4.9. Applicability in Monopolar Mode

In the event of a permanent single-pole-to-ground fault, the bipolar HVDC system can be restarted and operated through the healthy pole, i.e., in the monopolar mode with the ground return. Whenever the HVDC system restarts in the monopolar mode, the applied plan needs to be modified accordingly because measurable signals and output classes will differ from the bipolar mode.

A modified version of the proposed protection plan can be particularly prepared and trained for the monopolar mode. The following modifications should be applied to achieve this, assuming that the system structure in the monopolar mode includes the positive pole and the ground return path:

- A binary SVM classifier should be trained instead of the multiclass one since there will be only two output classes in this operational mode, including normal condition or external fault (i.e., 'Norm. or Ext.') and internal p-g fault (i.e., 'p-g').
- Instead of the four features introduced, only two features extracted from the positive pole voltage and DCF current signals (i.e., fe_1 and fe_3 extracted using (1) and (3), respectively) should be considered as inputs.

As can be comprehendible from the above modifications, the protection plan particularly prepared and trained for the monopolar mode will be much simpler than the one introduced in Section 3 for the normal bipolar mode.

4.10. Comparison to Other Intelligent plans

Table 7 compares the proposed plan to other intelligent plans designed so far to protect CSC-HVDC transmission systems. As can be understood from this table, although the proposed plan has a slightly higher delay than the one presented in [20], it has a superior ability to discriminate between external and internal faults. The proposed plan has less complexity compared to [20] and [21] since it detects and classifies internal faults in one step. The proposed plan's straightforward training and hyperparameter regulation procedures are significant advantages that make it superior to the plan designed in [21]. The proposed plan has a slightly lower delay than the plans presented in [21] and [22]. Moreover, unlike the plan presented in [22], the proposed plan does not require sending the fault detection and classification results to the rectifier station since it works based on the local measurements at the same station. It can be comprehended that the proposed plan is an effective step in improving intelligent protection strategies for CSC-HVDC transmission systems.

Table 7 Comparison with other intelligent protection plans designed for CSC-HVDC systems

Designed plan	Measuring end	No need for a telecommunication link	Fault detection and classification in one step	Discrimination ability between external and internal faults	Straightforward training and hyperparameter regulation procedures	Average FDTD (ms)
[20]	Rectifier	✓	×	×	✓	2.7*
[21]	Rectifier	✓	×	✓	×	5.7*
[22]	Inverter	×	✓	✓	✓	10.1*
Proposed	Rectifier	✓	✓	✓	✓	5

*Obtained by averaging the provided fault detection results in the reference

5. Conclusion

An efficient protection plan has been designed for bipolar CSC-HVDC transmission lines, using four useful features extracted from the locally measured voltage and DCF current samples and employing a multiclass SVM classifier. This plan has been evaluated in a typical 1000-km CSC-HVDC transmission system under a wide variety of conditions not seen in the training stage. The evaluation findings are as follows:

- The designed plan has quickly detected and correctly classified 100% of 1728 unseen solid and high-resistance line faults with an average FDTD of 5 ms.
- The proposed plan has remained stable against 99.375% of 1760 unseen external faults in the connected HVAC systems.
- The designed plan has performed satisfactorily under reasonable noise levels, even with an SNR of 20 dB.
- The proposed plan has remained stable during lightning strikes on the ground wire and pole conductors.
- The designed plan has performed satisfactorily in 2 out of 3 conductor interruption scenarios.

Comparisons confirm that this research provides a significant advance in developing intelligent protection strategies for CSC-HVDC systems. The proposed plan only requires single-end measurements and does not need data transmission or synchronization. Moreover, it works with a low signal sampling rate of 2 kHz, which is much lower than the required rates in the single-ended traveling-wave-based plans.

Acknowledgments

This work was supported by the Gonbad Kavous University [Research project ID: 6-195].

References

[1] M. Eremia, C.-C. Liu, A.-A. Edris, Advanced Solutions in Power Systems: HVDC, FACTS, and Artificial Intelligence, in, John Wiley & Sons, Hoboken, NJ, USA, 2016. https://doi.org/10.1002/9781119175391

[2] J. Liu, N. Tai, C. Fan, Y. Yang, Transient measured impedance-based protection scheme for DC line faults in ultra high-voltage direct-current system, IET Gener. Transm. Distrib., 10 (2016) 3597-3609. https://doi.org/10.1049/iet-gtd.2016.0408

[3] F. Kong, Z. Hao, S. Zhang, B. Zhang, Development of a novel protection device for bipolar HVDC transmission lines, IEEE Trans. Power Deliv., 29 (2014) 2270-2278. https://doi.org/10.1109/TPWRD.2014.2305660

[4] J. Suonan, J. Zhang, Z. Jiao, L. Yang, G. Song, Distance protection for HVDC transmission lines considering frequency-dependent parameters, IEEE Trans. Power Deliv., 28 (2013) 723-732. https://doi.org/10.1109/TPWRD.2012.2232312

[5] J. Zheng, M. Wen, Y. Chen, X. Shao, A novel differential protection scheme for HVDC transmission lines, Int. J. Electr. Power Energy Syst., 94 (2018) 171-178. https://doi.org/10.1016/j.ijepes.2017.07.006

[6] F. Kong, Z. Hao, B. Zhang, Improved differential current protection scheme for CSC-HVDC transmission lines, IET Gener. Transm. Distrib., 11 (2017) 978-986. https://doi.org/10.1049/iet-gtd.2016.0995

[7] S. Gao, Q. Liu, G. Song, Current differential protection principle of HVDC transmission system, IET Gener. Transm. Distrib., 11 (2017) 1286-1292. https://doi.org/10.1049/iet-gtd.2016.1380

[8] X. Chu, Transient numerical calculation and differential protection algorithm for HVDC transmission lines based on a frequency-dependent parameter model, Int. J. Electr. Power Energy Syst., 108 (2019) 107-116. https://doi.org/10.1016/j.ijepes.2018.12.039

[9] X. Chu, Unbalanced current analysis and novel differential protection for HVDC transmission lines based on the distributed parameter model, Electr. Power Syst. Res., 171 (2019) 105-115. https://doi.org/10.1016/j.epsr.2019.02.003

[10] Y. Zhang, Y. Li, J. Song, B. Li, X. Chen, A new protection scheme for HVDC transmission lines based on the specific frequency current of dc filter, IEEE Trans. Power Deliv., 34 (2019) 420-429. https://doi.org/10.1109/TPWRD.2018.2867737

[11] J. Zheng, M. Wen, Y. Qin, X. Wang, Y. Bai, A novel pilot directional backup protection scheme based on transient currents for HVDC lines, Int. J. Electr. Power Energy Syst., 115 (2020) 105424. https://doi.org/10.1016/j.ijepes.2019.105424

[12] Y. Li, Y. Zhang, J. Song, L. Zeng, J. Zhang, A novel pilot protection scheme for LCC-HVDC transmission lines based on smoothing-reactor voltage, Electr. Power Syst. Res., 168 (2019) 261-268. https://doi.org/10.1016/j.epsr.2018.12.012

[13] Y. Zhang, Y. Li, J. Song, X. Chen, Y. Lu, W. Wang, Pearson correlation coefficient of current derivatives based pilot protection scheme for long-distance LCC-HVDC transmission lines, Int. J. Electr. Power Energy Syst., 116 (2020) 105526. https://doi.org/10.1016/j.ijepes.2019.105526

[14] D. Wang, H.L. Gao, S.B. Luo, G.B. Zou, Travelling wave pilot protection for LCC-HVDC transmission lines based on electronic transformers' differential output characteristic, Int. J. Electr. Power Energy Syst., 93 (2017) 283-290. https://doi.org/10.1016/j.ijepes.2017.06.004

[15] J. Wu, H. Li, G. Wang, Y. Liang, An improved traveling-wave protection scheme for LCC-HVDC transmission lines, IEEE Trans. Power Deliv., 32 (2017) 106-116. https://doi.org/10.1109/TPWRD.2016.2549565

[16] W. Hao, S. Mirsaeidi, X. Kang, X. Dong, D. Tzelepis, A novel traveling-wave-based protection scheme for LCC-HVDC systems using Teager Energy Operator, Int. J. Electr. Power Energy Syst., 99 (2018) 474-480. https://doi.org/10.1016/j.ijepes.2018.01.048

[17] F. Kong, Z. Hao, B. Zhang, A novel traveling-wave-based main protection scheme for ±800 kV UHVDC bipolar transmission lines, IEEE Trans. Power Deliv., 31 (2016) 2159-2168. https://doi.org/10.1109/TPWRD.2016.2571438

[18] Y. Ma, H. Li, G. Wang, J. Wu, Fault analysis and traveling-wave-based protection scheme for double-circuit LCC-HVDC transmission lines with shared towers, IEEE Trans. Power Deliv., 33 (2018) 1479-1488. https://doi.org/10.1109/TPWRD.2018.2799323

[19] D. Marques da Silva, F.B. Costa, V. Miranda, H. Leite, Wavelet-based analysis and detection of traveling waves due to DC faults in LCC HVDC systems, Int. J. Electr. Power Energy Syst., 104 (2019) 291-300. https://doi.org/10.1016/j.ijepes.2018.07.011

[20] J.M. Johnson, A. Yadav, Complete protection scheme for fault detection, classification and location estimation in HVDC transmission lines using support vector machines, IET Sci. Meas. Technol., 11 (2017) 279-287. https://doi.org/10.1049/iet-smt.2016.0244

[21] S. Agarwal, A. Swetapadma, C. Panigrahi, A. Dasgupta, A method for fault section identification in High voltage direct current transmission lines using one End measurements, Electr. Power Syst. Res., 172 (2019) 140-151. https://doi.org/10.1016/j.epsr.2019.03.008

[22] M. Farshad, Detection and classification of internal faults in bipolar HVDC transmission lines based on K-means data description method, Int. J. Electr. Power Energy Syst., 104 (2019) 615-625. https://doi.org/10.1016/j.ijepes.2018.07.044

[23] W.A. Woyczyński, Stationary Signals, in: A First Course in Statistics for Signal Analysis, Birkhäuser Boston, Boston, 2011, pp. 105-125. https://doi.org/10.1007/978-0-8176-8101-2_4

[24] T.V. Prasad, S.I. Ahson, Data Mining for Bioinformatics — Microarray Data, in: M.H. Fulekar (Ed.) Bioinformatics: Applications in Life and Environmental Sciences, Springer Netherlands, Dordrecht, 2009, pp. 77-144. https://doi.org/10.1007/978-1-4020-8880-3_8

[25] M. Szechtman, T. Margaard, J.P. Bowles, C.V. Thio, D. Woodford, T. Wess, R. Joetten, G. Liss, M. Rashwan, P.C. Krishnayya, P. Pavlinec, V. Kovalev, K. Maier, J. Gleadow, J.L. Haddock, N. Kaul, R. Bunch, R. Johnson, G. Dellepiane, N. Vovos, The CIGRE HVDC benchmark model–a new proposal with revised parameters, Electra, (1994) 61-65.

[26] B. Scholkopf, C. Burges, A. Smola, Advances in Kernel Methods - Support Vector Learning, in, MIT Press, Cambridge, MA, USA, 1999.

[27] S. Escalera, O. Pujol, P. Radeva, On the decoding process in ternary error-correcting output codes, IEEE Trans. Pattern Anal. Mach. Intell., 32 (2010) 120-134. https://doi.org/10.1109/TPAMI.2008.266

[28] S. Abe, Support Vector Machines for Pattern Classification, Springer-Verlag, London, UK, 2005.

[29] PSCAD/EMTDC User's Guide, in, Manitoba HVDC Research Ctr., Winnipeg, MB, Canada, 2005.

[30] M. Farshad, Locating short-circuit faults in HVDC systems using automatically selected frequency-domain features, Int. Trans. Electr. Energy Syst., 29 (2019) e2765. https://doi.org/10.1002/etep.2765

[31] MATLAB User's Guide: R2018b Documentation, in, MathWorks Inc, Natick, MA, USA, 2018.

[32] D. Tzelepis, V. Psaras, E. Tsotsopoulou, S. Mirsaeidi, A. Dyśko, Q. Hong, X. Dong, S.M. Blair, V.C. Nikolaidis, V. Papaspiliotopoulos, G. Fusiek, G.M. Burt, P. Niewczas, C.D. Booth,

Voltage and current measuring technologies for high voltage direct current supergrids: a technology review identifying the options for protection, fault location and automation applications, IEEE Access, 8 (2020) 203398-203428. https://doi.org/10.1109/ACCESS.2020.3035905

[33] D. Muthumuni, L. Kothalawala, A. Darbandi, Lightning Studies, Manitoba HVDC Research Ctr., Winnipeg, MB, Canada, 2016. https://www.pscad.com/knowledge-base/download/lightning_studies_20160908.pdf [Accessed: May 2021]

[34] W. Jia, Z. Xiaoqing, Double-exponential expression of lightning current waveforms, in: The 2006 4th Asia-Pacific Conference on Environmental Electromagnetics, 2006, pp. 320-323. https://doi.org/10.1109/CEEM.2006.257962